Effect of Xe dilution on structural, electrical and optical properties of nanocrystalline Si films deposited by HW-CVD method

Vaishali S. Waman[1, 2], Azam H. Mayabadi[1], Mahesh M. Kamble[1], Bharat B. Gabhale[1], Adinath M. Funde, Vasant G. Sathe[3], Habib M. Pathan[4], Sandesh R. Jadkar[4*]

[1]Modern College of Arts, Science and Commerce, Shivajinagar, Pune 411005, India
[2]School of Energy Studies, Savitribai Phule Pune University, Pune 411007, India
[3]UGC-DAE-CSR, University Campus, Khandawa Road, Indore 452017, India
[4]Department of Physics, Savitribai Phule Pune University, Pune 411007, India

[*]Corresponding author. Tel: (+91)-20-2569 2678; E-mail: sandesh@physics.unipune.ac.in

ABSTRACT

We investigated the effect of Xe dilution of silane on structural, optical and electrical properties of nanocrystalline Si films deposited by HW-CVD. With increase in Xe dilution of silane nanocrystalline-to-amorphous transition or amorphization has been observed in nanocrystalline Si films. The amorphization has been confirmed from dark and photoconductivity measurement, Raman spectroscopy, low angle XRD and atomic force microscopy analysis. The FTIR spectroscopy analysis showed that with increase in Xe dilution of silane, in addition to di-hydrogen [$Si-H_2$] and poly-hydrogen [$(Si-H_2)_n$] complexes, hydrogen incorporated in these films in mono-hydrogen [$Si-H$] bonded species. The hydrogen content was found < 5 at. % over the entire range of Xe dilution of silane studied and it increases with increase in Xe dilution of silane. On the other hand, E_{Tauc} and E_{04} show decreasing trend with increasing Xe dilution of silane. The E_{Tauc} decreases from 2.4eV to 1.9eV whereas E_{04} decreases from 2.9eV to 2.3eV. The optical band gap values estimated from E_{04} method are found higher than E_{Tauc} values calculated from Tauc's method. Finally, it has been concluded that Xe dilution of silane in HW-CVD enhances the deposition rate but has adverse effect on the crystallinity of nanocrystalline Si films. Copyright © 2015 VBRI Press.

Keywords: Optical properties of thin films; raman spectra of semiconductors; x-ray diffractometers; electrical properties of films; chemical vapor deposition.

Introduction

Over the last few decades hydrogenated amorphous silicon (a-Si:H) has been studied extensively as a basic material for thin film solar cells. However, solar cells based on a-Si:H have always been associated with efficiency losses due to the light-induced degradation with time [1]. Nowadays, a-Si:H has been replaced hydrogenated nanocrystalline silicon (nc-Si:H) due to its vital properties such as high conductivity, high charge carrier mobility and high doping efficiency [2] which has lead to upsurge in interest pertaining to potential applications such as solar cells [3, 4], photodiodes [5] and thin film transistors [6]. Of late, nc-Si:H films have been reported to have an improved stability against prolonged light illumination [7-9] that portrays it as attractive candidates to improve both the efficiency and the stability of solar cells and other opto-electronic devices.

Several deposition methods such as pulse laser deposition (PLD) [10], plasma enhanced chemical vapor deposition (PE-CVD) [11], electron cyclotron resonance plasma enhanced CVD (ECR-PE-CVD) [12], sputtering [13] etc. have been employed to deposit nc-Si:H films with good opto-electronic properties. However, only plasma enhanced chemical vapor deposition (PE-CVD) has been established for the industrial applications. The high H_2 dilution of silane and high radio frequency (RF) power to silane plasma are two critical parameters that facilitate the growth of nc-Si:H in PE-CVD. The high H_2 dilution retards the deposition rate whereas use of high RF power has adverse effect on transparent conducting coating on which solar cell is fabricated. For device fabrication both these events are undesirable. Various inert gases like helium (He) [14], argon (Ar) [15] and xenon (Xe) [16] have been used in PE-CVD for dilution of silane to deposit Si:H films at low substrate temperature with increased the deposition rates. These gases have shown strong influence on the structure and morphology of the films.

The hot wire chemical vapor deposition (HW-CVD) or simply 'hot-wire method' has received considerable attention in recent years as an alternative deposition method for nc-Si:H owing to its capability to form stable films [17] and of achieving higher deposition rates [18]. The method has been employed successfully for the synthesis of new

microcrystalline materials like μc-SiC and μc-GeC for solar cell applications [**19**]. So far, the influence of xenon dilution of silane in HW-CVD has still not been studied and no reports exist in the literature. With this motivation an attempt have been made to ascertain the role of Xe dilution of silane ($R_{Xe} = F_{Xe}/F_{SiH4} + F_{Xe}$) on structural, optical and electrical properties of Si:H films deposited by HW-CVD. Here, F_{Xe} and F_{SiH4} are xenon and silane gas flow rates, respectively. In this paper, we present the investigation of structural, optical and electrical properties of nanocrystalline Si films deposited by HW-CVD from Xe dilution of SiH_4 without hydrogen. It has been observed that addition of Xe with silane in HW-CVD has adverse effect on crystallinity of nanocrystalline Si films.

Experimental

Material synthesis

Fig. 1 shows the schematic of indigenously designed and locally fabricated dual chamber hot wire chemical vapor deposition (HW-CVD) unit used for the synthesis of nc-Si:H films in the present study. It consists of two stainless steel chambers, referred as process chamber and load lock chamber. The process chamber is coupled with a turbo molecular pump which yields a base pressure less than 10^{-6} Torr. Use of load lock chamber prevents the process chamber to be directly exposed to air, which minimizes the pump down time and reduce contamination of layers with oxygen and water vapors. Substrates can be moved from load lock to process chamber using pneumatically controlled transport system.
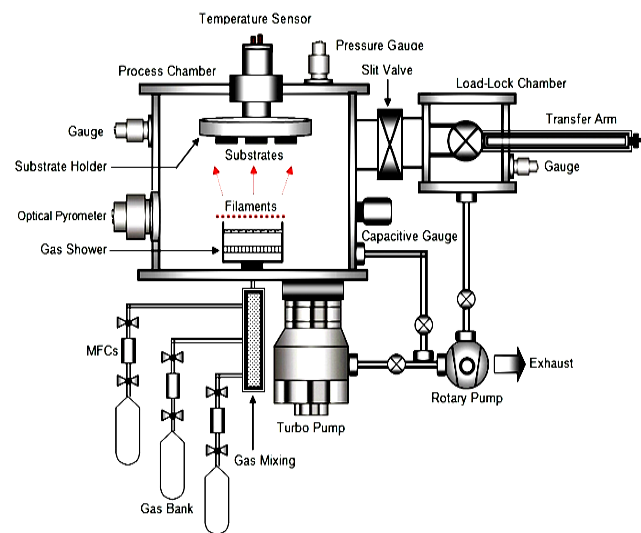

Fig. 1. Schematic of indigenously designed and locally fabricated dual chamber hot wire chemical vapor deposition (HW-CVD) unit used for the synthesis of nc-Si:H films.

The pressure during deposition was kept constant (50 mTorr) by using automated throttle valve. For deposition we have used 10 straight W filaments, 1 cm apart mounted parallel to each other. Each filament has a diameter of 0.5 mm and a length of 10 cm. Heating of filaments is done by an AC current using a current transformer and dimmer. The filament temperature was kept constant and measured by optical pyrometer. A shutter is placed in front of the substrates to shield the substrates from undesired deposition during pre-heating of filaments. Reaction gases were introduced in the process chamber from the bottom and perpendicular to the plane of filaments through a specially designed gas shower to ensure uniform gas flow over the filaments. The substrates can be placed on substrate holder which is heated by in build heater using K type thermocouple (chromel-alumel) and temperature controller. Films were deposited using a mixture of pure silane (SiH_4) (Matheson Semiconductor Grade) and xenon (Xe) gases without hydrogen (H_2) dilution. Temperature of the filament and substrate was maintained at 1900 ^{0}C and at 200 ^{0}C respectively. The silane flow rate (F_{SiH4}) was kept constant at 5 sccm, while Xenon flow rate (F_{Xe}) was varied from 5 sccm to 50 sccm. The nc-Si:H thin films were deposited simultaneously on corning #7059 glass and c-Si wafers having dimensions 5 cm x 5 cm and 1 x 1 cm respectively.

Film characterization

Dark conductivity (σ_{dark}) and photoconductivity (σ_{photo}) was measured at room temperature employing a 2400 Keithley source-meter in planar geometry using the relation,

$$\sigma_{Dark(Photo)} = \left[\frac{V \times d \times \omega}{I_{Dark(Photo)} \times l} \right]^1 \quad (1)$$

where, V is applied voltage (volts), $I_{Dark(Photo)}$ is Dark (Photo) current (amperes), d is thickness (cm), ω is width (cm) and l is the distance between the electrodes (cm). For band gap estimation, transmission (T) and reflection (R) spectra were recorded using a double beam UV-Visible spectrophotometer (JASCO Model: V-670) having resolution 0.1 nm. Band gap was then determined by plotting the *Tauc's* curve. To determine the amount of bonded hydrogen and the hydrogen-bonding configuration in the film we have employed FTIR spectroscopy (JASCO spectrometer, Model V6100A) with a resolution of 0.4 cm^{-1} in the transmission (T) mode. The surface morphology and surface roughness of the films were investigated using non-contact mode atomic force microscopy (NC-AFM) (JEOL, JSPM-5200, Japan) having atomic scale resolution. Raman spectra were recorded with Jobin Yvon Horibra Raman spectroscopy in backscattering geometry with the resolution of 1 cm^{-1}. To estimate crystalline fraction (X_{Raman}) and crystallite size (d_{Raman}) the Raman spectra was de-convoluted into two Gaussian peaks and one Lorentzian peak with a quadratic base line method in the range 400-540 cm^{-1} using *Levenberg-Marquardt* method [**20**]. The crystalline fraction (X_{Raman}) was calculated using equation [**21**].

$$X_{Raman} = \frac{I_c + I_m}{I_c + I_m + I_a} \quad (2)$$

where, I_c is the integrated intensity of the crystalline phase near 520 cm^{-1}, I_m is the integrated intensity of the intermediate phase around 500 cm^{-1} and I_a is the integrated intensity of the amorphous phase at 480 cm^{-1}. The crystallite size (d_{Raman}) was deduced using [**22**].

$$d_{Raman} = 2\pi\sqrt{\left(\frac{\beta}{\Delta\omega}\right)} \qquad (3)$$

where, $\Delta\omega$ is the peak shift compared to c-Si peak located $\sim$ 520 cm^{-1} and β = 2.0 cm^{-1}nm^2. The X-ray diffraction pattern was obtained by Bruker D8 Advance x-ray diffractometer at a grazing angle of 1^0 with scan step size 0.1^0 and speed of speed 5 sec/step. The average crystallite size was estimated using the *Scherer's* formula [23].

$$d_{x-ray} = \frac{0.9\,\lambda}{(\beta\cos\theta_B)} \qquad (4)$$

where, λ is the wavelength of diffracted radiation, θ_B is the Bragg angle and β is the line width (FWHM) in radians. Thickness of films was determined by profilometer (KLA Tencor, P-16+) and further confirmed by UV-Visible spectroscopy using the method proposed by Swanepoel [24].

Results and discussion

Variation of deposition rate

Films were deposited for a fixed time period and the deposition rate is calculated from thickness measurement. The variation of deposition rate (r_d) as a function of Xe dilution of silane (R_{Xe}) is shown in **Fig. 2**. As seen from the figure, the deposition rate increases from 12 Å/s to 15.2 Å/s when R_{Xe} increases from 0 % (No Xe dilution of SiH$_4$) to 91 %. The increase in the deposition rate with increase in Xe dilution of silane was reported previously for PE-CVD deposited Si:H and diamond films [25, 26].
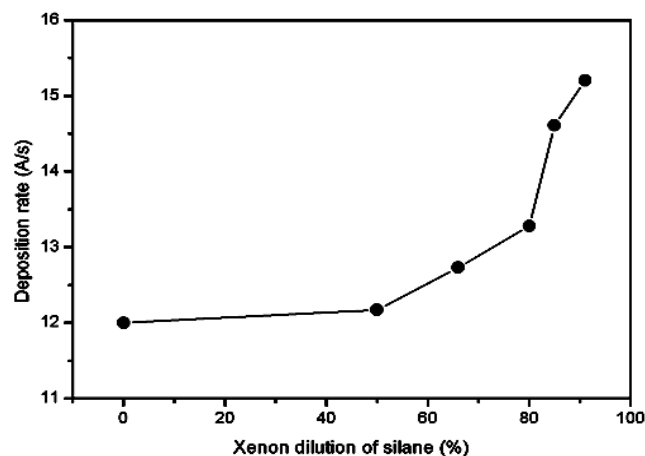
Fig. 2. Variation of deposition rate as function of Xe dilution of silane for the Si:H films deposited by HW-CVD method.

Electrical properties

The variation of the dark conductivity (σ_{Dark}) and the photoconductivity (σ_{Photo}) are shown as a function of Xe dilution of silane (R_{Xe}) in **Fig. 3**. Data in **Fig. 3** shows that the film deposited at R_{Xe} = 0 % (No Xe dilution of SiH$_4$)

both, σ_{Dark} and σ_{Photo} are almost have same values ($\sim 10^{-6}$ S/cm). As a result, photosensitivity gain, taken as the ratio of photoconductivity-to-dark conductivity (σ_{Photo} /σ_{Dark}) is $\sim$1. This is typical feature of nanocrystalline Si (nc-Si:H) films because the nc-Si:H films prepared by different methods show high dark conductivity and negligible photosensitivity gain depending upon the crystallite size and its volume fraction [27]. With increase in R_{Xe}, the σ_{Dark} decreases by four order of magnitude (from $\sim 4\times10^{-6}$ S/cm to $\sim 7\times10^{-10}$ S/cm) whereas σ_{Photo} remains approximately constant (10^{-5} S/cm) for the entire range of R_{Xe} studied. As a result, the photosensitivity gain increases from 10^0 to 10^5 when R_{Xe} increased from 0 % to 91 %. It should also be noted that the photosensitivity gain for R_{Xe} = 91 % film is more than 5 orders magnitude which is typical of device quality a-Si:H material grown by PE-CVD. These results indicate that the films deposited with increasing Xe dilution of silane get structurally modified. We attribute the drastic enhancement in photosensitivity to nanocrystalline-to-amorphous transition or amorphization in the films with increase in R_{Xe}. The evidence of gradual nanocrystalline-to-amorphous transition with increasing Xe dilution of silane comes from Raman spectroscopy and low angle XRD and atomic force microscopy (AFM) analysis.
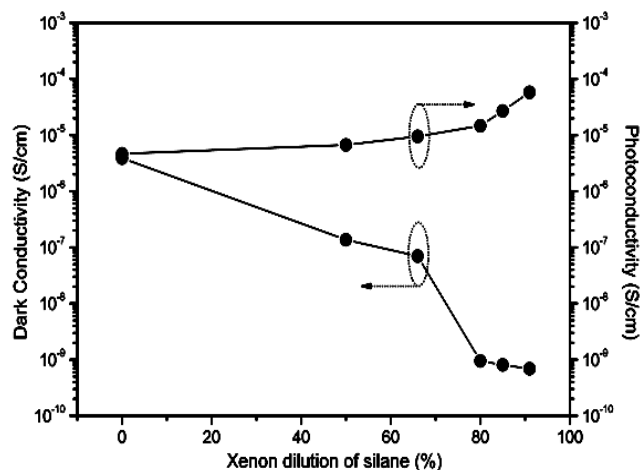
Fig. 3. Variation in dark conductivity and photoconductivity as a function of Xe dilution of silane.

Low angle x-ray diffraction (XRD) analysis

To identify the crystallinity in the films low angle x-ray diffraction (XRD) studies were performed. The low angle XRD pattern of Si:H films deposited at different Xe dilution of silane (R_{Xe}) are shown in **Fig. 4**. The average crystallite size (d_{x-ray}), deduced using Debye-Scherrer's formula are also indicated in the figure. It is evident from the figure that the film deposited at R_{Xe}= 0 % is nanocrystalline Si, having three peaks at $2\theta \sim 28.4^0$, 47.4^0 and 56.1^0 corresponding to (111), (220) and (311) crystal orientations, respectively. The dominant peak is (111), indicating that the crystallites have preferential orientation in (111) direction. However, the films deposited with increasing R_{Xe}, the diffraction peaks corresponding to all the crystallographic planes were found to decrease, both in intensity and sharpness suggesting decrease in its volume fraction of crystallites and its size. It is interesting to note

that the films deposited at higher Xe dilution of silane (R_{Xe} = 85 % and 91 %) all crystallographic planes disappears and a broad hump at $2\theta \sim 27^0$ emerge in the XRD pattern indicating that films are amorphous. Thus, addition of Xe with silane in HW-CVD induces amorphization in nanocrystalline Si film structure. These results are consistent with the Raman results (discussed later).
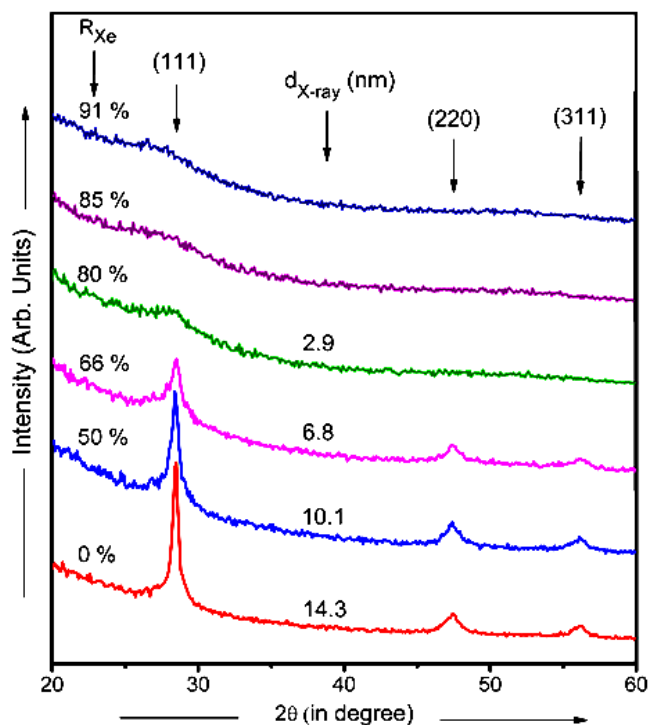

Fig. 4. Low angle XRD pattern of films deposited by HW-CVD at different Xe dilution of silane.

Raman spectroscopy analysis

Raman spectroscopy is a non-destructive tool of analysis which provides direct structural information quantitatively related to the average crystallite size and the crystalline volume fraction in the film. **Fig. 5** shows the Raman spectra of Si:H films deposited at various Xe dilution of silane (R_{Xe}). To estimate the crystalline fraction (X_{Raman}) and crystallite size (d_{Raman}) each spectrum shown in **Fig. 5** was de-convoluted into two Gaussian peaks and one Lorentzian peak with a quadratic base line method mentioned in the experimental section. The estimated crystalline fraction (X_{Raman}) and crystallite size (d_{Raman}) in the film are also indicated in the **Fig. 5**. Following observations have been made from the Raman spectra for Si:H films deposited at various Xe dilution of SiH_4.

1) Films deposited at R_{Xe} = 0 % (No Xe dilution of SiH_4), the Raman spectra show a sharp peak centered ~ 517.5 cm^{-1} corresponding to transverse optical (TO) vibrational mode of nanocrystalline Si [28]. For this film crystalline fraction (X_{Raman}) is 81.3 % and crystallite size (d_{Raman}) is 4.8 nm.
2) When small amount of Xe is added with silane (film deposited at R_{Xe} = 50 %), the nanocrystalline Si TO Raman peak shifts towards the lower wave number 516.0 cm^{-1} and its intensity decline. The shifting of TO

peak towards lower wave number indicates decrease in crystallite size whereas decline in intensity signify decrease in volume fraction of crystallites in the film.
3) Film deposited at R_{Xe} = 66 %, an additional broad shoulder centered ~ 490.0 cm^{-1} partially emerged in the Raman spectra which corresponds to TO vibrational mode of amorphous Si (a-Si:H) suggesting the mixed phase of amorphous and nanocrystalline Si [29].
4) With further increase in R_{Xe}, the nanocrystalline Si TO peak shift further towards the lower wave number. At the same time, the amorphous Si TO peak predominately appears ~ 480.0 cm^{-1} with enhanced intensity.
5) Finally, the films deposited at R_{Xe} = 85 % and 91 %, the nanocrystalline Si TO peak completely disappear and a broad shoulder ~ 470 cm^{-1} can be seen in the spectra which is characteristic feature of a-Si:H.
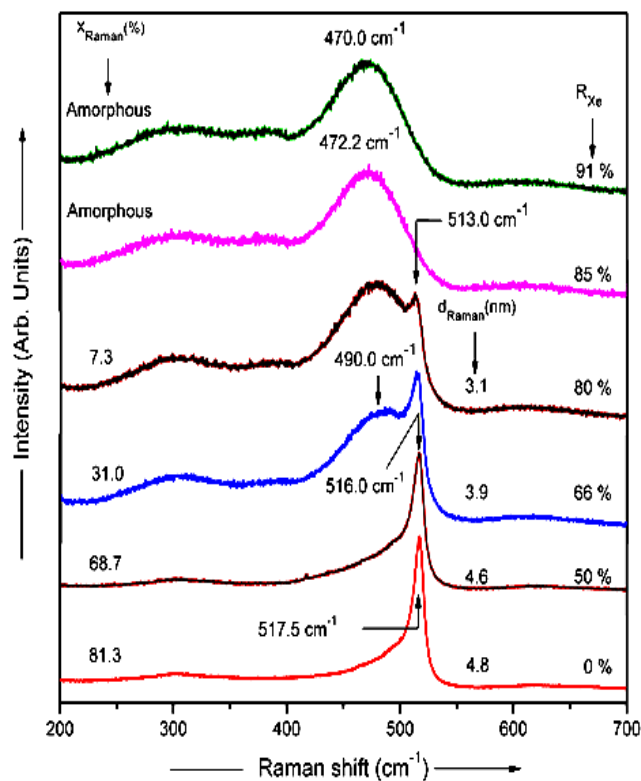

Fig. 5. Raman spectra of films deposited at various Xe dilution of silane using HW-CVD.

These results indicate that Xe dilution of silane induces amorphization in nanocrystalline Si film structure. These results are in consistent with the low angle XRD analysis. It has been reported that Xe ion bombardment is beneficial in enhancing high quality silicon film growth in PE-CVD [30, 31]. In HW-CVD, at the filament temperature 1900 ^{0}C the thermal energy available is ~ 0.25 eV [32] and the ionization energy of Xe atom is very high (12.13 eV) [33]. Therefore, the possibility of formation of metastable state of xenon atoms (Xe^*) and xenon ions (Xe^+) responsible for quality silicon film growth in HW-CVD is negligible compared to conventional PE-CVD. As a result, the energy required for the formation of nano-crystals in the amorphous network (called Gibb's free energy for crystallization) [34] is not available in the growth zone

using Xe dilution of SiH$_4$. We think that due to the large mass the Xe atoms may receive thermal energy from the heater and the electrons emitted by hot tungsten (W) filaments [**35**]. With increasing Xe dilution, the density of thermal Xe atoms in the vicinity of growth zone increases. This increases the collision of thermal Xe atoms with the growing surface. The impingement of thermal Xe atoms may modify the growing surface which results the transform in film structure from crystalline to amorphous with increase in Xe dilution of SiH$_4$. Furthermore, the abundance of atomic H on, or near, the growing surface plays an important role in the formation of nc-Si:H films. These energetic atomic H may penetrate into layers below the top surface of the film [**36**] and promotes the network propagation reaction by dangling bond compensation, weak bond breaking and reconstruction of strong Si-Si bonds, strain relaxation, and giving chemical potential to the growing surface by breaking the Si-H bond, thereby leading to structural reorientation for attaining energetically favorable configuration and hence nanocrystallization. In addition, atomic H radicals act as an etchant of Si atoms from the weak Si-Si bonds at the growing surface and which further promote the nanocrystallization when chemical equilibrium between deposition and etching is attained. However, with increase in Xe dilution of SiH$_4$ the density of atomic H on/near, the growing surface substantially gets reduced. Thus, the lack of atomic H at the growing surface may be another possible reason for amorphization. The increase in deposition rate with increase in Xe dilution of of SiH$_4$ supports this conjecture (**Fig. 1**).

Atomic force microscopy (AFM) analysis

Non-contact AFM images of Si:H films deposited at Xe dilution of SiH$_4$ (R$_{He}$)= 0 %, 50 % and 91 %, by HW-CVD method are shown in **Fig. 6**. With change in Xe dilution of SiH$_4$, significant differences in the structure can be clearly seen. The AFM micrograph for the film deposited at R$_{Xe}$ = 0 % [**Fig. 6(a)**] clearly reveals well resolved, large number of uniform nanocrystallites embedded in the amorphous matrix. Each crystallite has an individual identity with its size in the range ~ 80-90 nm and rms surface roughness ~ 2.21 nm. The film deposited at R$_{Xe}$ = 50 % [**Fig. 6(b)**] indicate decrease in density of nanocrystallites and it looks like the smaller grains form into clusters, that is they agglomerates. For this film the average grain size is in the range ~ 60-90 nm and rms surface roughness ~ 2.94 nm. Difference between the average grain size determined by XRD and Raman spectroscopy and AFM techniques has been reported previously [**37**]. Almost complete disappearance of nanocrystalline phase can be clearly seen in the AFM image for the film deposited at R$_{Xe}$ = 91 % [**Fig. 6(c)**]. Along with Raman and low angle XRD analysis the AMF analysis further give clear evidence of nanocrystalline-to-amorphous transition in films with increase in Xe dilution of SiH$_4$.
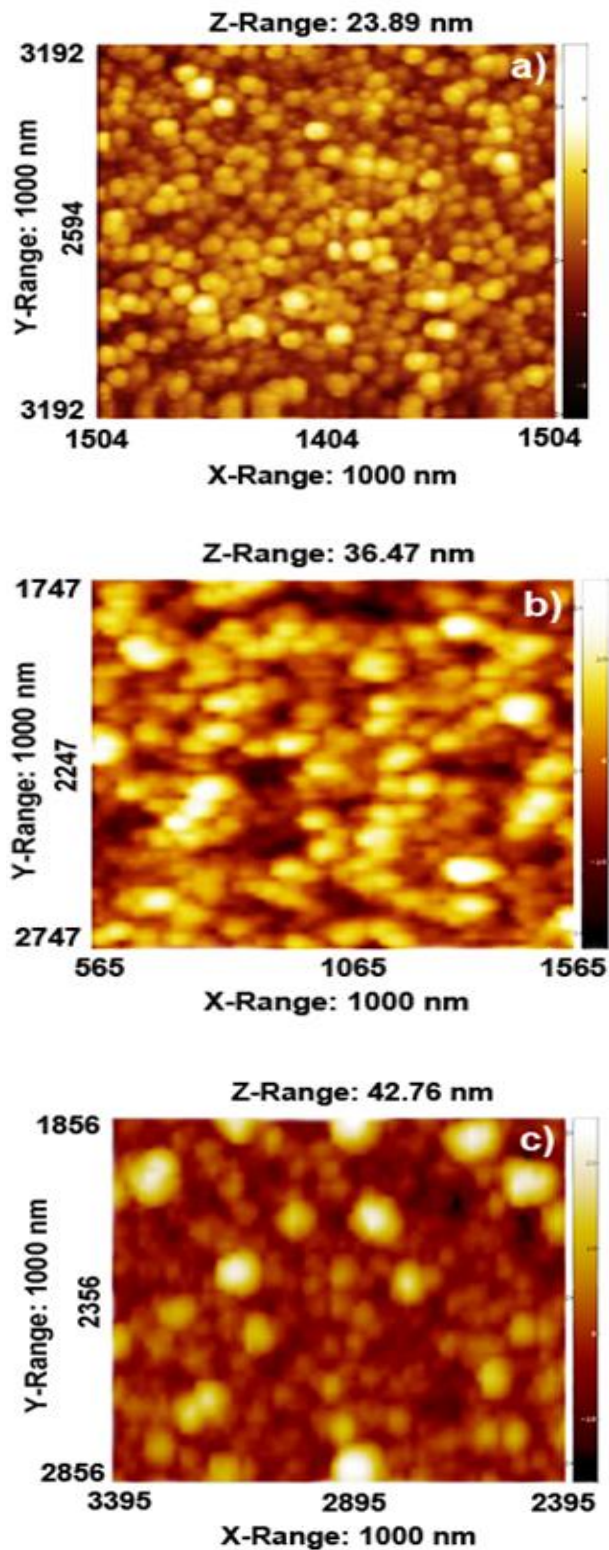

Fig. 6. Non-contact atomic force microscopy (NC-AFM) images of films deposited at various Xe dilution of silane (a) R$_{Xe}$ = 0 %, (b) R$_{Xe}$ = 50 %, and (c) R$_{Xe}$ = 91 %, by HW-CVD method.

Fourier transform infra-red (FTIR) spectroscopy analysis

To investigate the effect of Xe dilution of SiH$_4$ on Si-H bonding configuration and to determine the bounded hydrogen content, Fourier transform infrared (FTIR) spectroscopy was used. The FTIR spectra (normalized for

thickness) of Si:H films deposited by HW-CVD method at different Xe dilution of silane (R_{Xe}) are shown in **Fig. 7**. For clarity, the spectra have been broken horizontally into two parts. It can be seen from the spectra for the film deposited at no Xe dilution i. e. $R_{Xe}= 0$ %, have three major absorption bands at ~ 630 cm^{-1}, ~ 880 cm^{-1} and ~ 2100 cm^{-1} corresponding to the wagging vibrational modes of different bonding configurations, the scissor bending mode of polymerized $(Si-H_2)_n$ bonded species and the stretching vibrational modes of di-hydrogen species $(Si-H_2)$ and poly-hydrogen $(Si-H_2)_n$ complexes (isolated or coupled), respectively [**38-40**]. Thus, the film deposited without Xe dilution of SiH_4, the hydrogen incorporated mainly in di-hydrogen species $(Si-H_2)$ and poly-hydrogen $(Si-H_2)_n$ bonded species. The films deposited at similar growth rates at various Xe dilution of silane show similar bands, but with additional absorption peak ~ 2000 cm^{-1} and its intensity increases with increase in R_{Xe}. According to the literature the absorption peak ~ 2000 cm^{-1} corresponds to wagging vibrational mode of mono-hydrogen (Si-H) bonded species [**38-40**]. These results suggest that besides $Si-H_2$ and $(Si-H_2)_n$ bonding species, with increase in Xe dilution of silane, the hydrogen also incorporated in the in the film in Si-H bonded species.
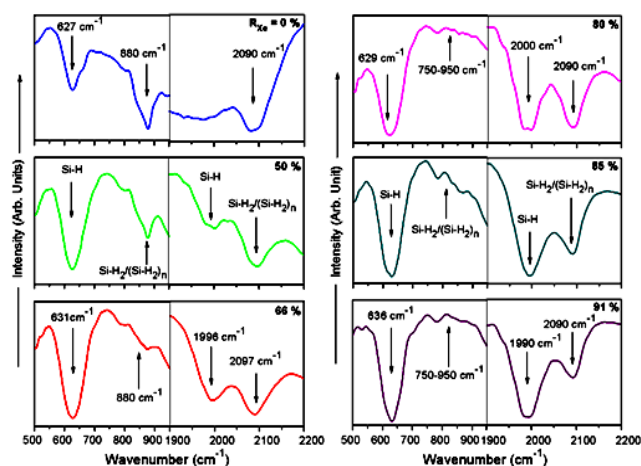
Fig. 7. FTIR spectra showing the H-related features of nanocrystalline Si films (normalized to thickness) deposited by HW-CVD at different Xe dilution of silane.

It was found that the hydrogen content in Si:H materials calculated from different methods is quite different. However, it has been reported that the integrated intensity of the peak ~ 630 cm^{-1} is the best measure of hydrogen content and other bands are less reliable [**41**] and whatever may be the nature of the hydrogen bonding configuration, Si-H, $Si-H_2$, $(Si-H_2)_n$, SiH_3, and so forth, all types of the vibrational modes will contribute to the 630 cm^{-1} absorption band [**42**]. Thus, the total bonded hydrogen atoms (C_H) has been estimated from integrated intensity of the peak at 630 cm^{-1} using relation.

$$C_H \text{ (at. \%)} = \frac{A_H}{N_{Si}} \int \frac{\alpha(\omega)}{\omega} d\omega \qquad (5)$$

where, $\alpha(\omega)$ is the absorption coefficient of the film at the wave number ω, $A = 1.6 \times 10^{19}$ cm^{-2} is a proportionality

constant which varies as the inverse of the oscillator strength [**43**] and $N_{Si} = 5 \times 10^{22}$ cm^{-3} is the atomic density of pure Si. **Fig. 8** shows the variation of hydrogen content (C_H) as a function of Xe dilution of silane (R_{Xe}). The hydrogen content in the film increases from 1.39 at. % to 4.66 at % when Xe dilution of silane increased from 0 % to 91 %. It is interesting to note that the total bonded hydrogen content is less than the 5 at. % over the entire range of Xe dilution of silane studied.
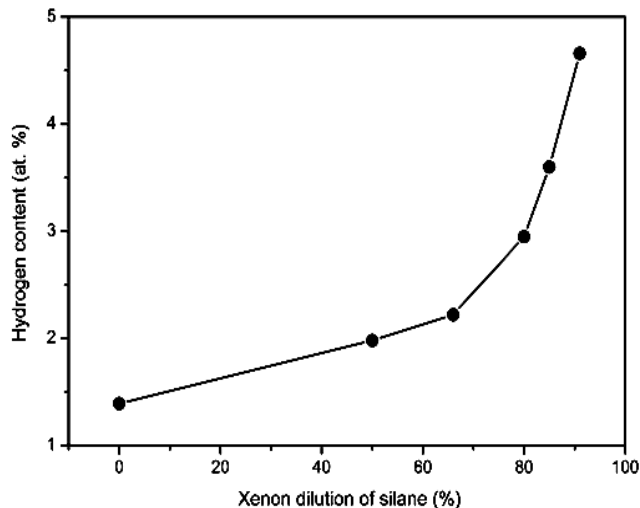

Fig. 8. Variation of hydrogen content nanocrystalline Si films deposited by HW-CVD as a function of xenon dilution of silane.

UV-Visible spectroscopy analysis

The absorption coefficient (α) was estimated from transmission (T) and reflection (R) spectra in the wavelength range of 200-900 nm. The α is calculated for each wavelength using the relation,

$$\alpha = -\frac{1}{d} \ln\left(\frac{T}{1-R}\right) \qquad (6)$$

where, t is the thickness of film. The optical band gap (E_{opt}) of the film was then calculated from the dependence of the absorption coefficient (α) on the photon energy (hν) taking into account that Si:H as a semiconductor. For direct allowed transition, absorption coefficient (α) and band gap can be expressed as [**44**],

$$(\alpha E)^{1/2} = B^{1/2}(E - E_{Tauc}) \qquad (7)$$

where, B is an energy independent constant, E is the photon energy and E_{Tauc} is optical band gap. To determine the band gap, $(\alpha h\nu)^{1/2}$ is plotted against energy E (= hν). A straight line fitted through the data points. The line is then extrapolated and the intercept of the extrapolated line on the energy axis gives the optical band gap. It is agreed that the determination of band gap is not accurate using Tauc's formulation because of the extent of the valence and conduction band tails in the gap, especially in case of films where nanocrystallites are embedded in the amorphous matrix. However, it is expected to give an approximate estimate of the band gap. Thus, the energy where the

absorption coefficient (α) is equal to 10^{-4} cm^{-1}, designated E_{04}, is also obtained from the transmission measurements. **Fig. 9** show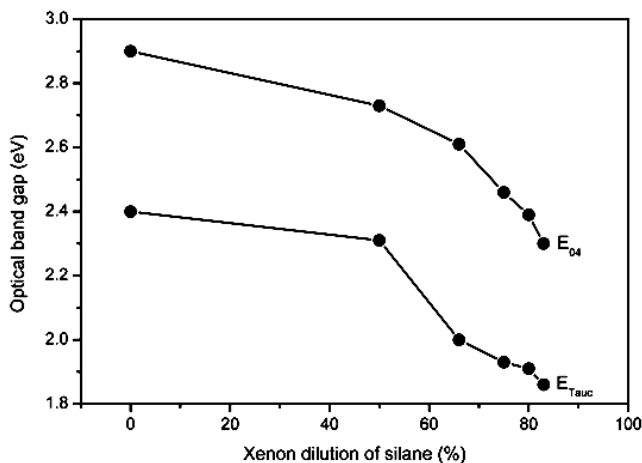s a comparison of E_{Tauc} and E_{04} as a function of Xe dilution of silane for the films deposited by HW-CVD method. It can be seen that both, E_{Tauc} and E_{04} show decreasing trend with increasing Xe dilution of silane. The E_{Tauc} decreases from 2.4eV to 1.9eV whereas E_{04} decreases from 2.9eV to 2.3eV when Xe dilution of silane increased from 0 % to 91 %. It is interesting to note that optical band gap values estimated from E_{04} method are found higher than E_{Tauc} values calculated from Tauc's method. It is generally accepted that the band gap of Si:H depends on the hydrogen content and it increases with the increase in hydrogen content in the films [**45**].

Fig. 9. Comparison of ETauc and E04 as a function of xenon dilution of silane for nanocrystalline Si films deposited by HW-CVD method.

The band gap linearly increases from 1.5 to 1.7eV when the hydrogen content in the film increases from 2 to 11 at. %. Then up to a hydrogen contents of 20 at. %, the band gap remains constant [**46, 47**]. However, in the present study, with increase in Xe dilution of silane the hydrogen content in the film increases (**Fig. 8**) whereas, the band gap shows decreasing trend. In fact the band gap remains as high as 1.9 eV even when the hydrogen content in the film is less than 5 at. %. Thus, the amount of bounded hydrogen only cannot account for the band gap in nanocrystalline Si films. In addition there are several ambiguities about the high band gap of nanocrystalline Si films because the material contains both phases, amorphous and crystalline and their properties vary with the volume fraction of these phases. Accordingly, in the case of a mixed phase the band gap should lie between amorphous and crystalline silicon [**48**]. The typical value of the band gap of a-Si:H is between 1.6 and 1.8eV depending on the process parameters. The high band gap of mixed phase nanocrystalline Si films has been attributed by various researchers to the hydrogen content [**45**], crystalline fraction [**14**], improvement of short and medium range order [**49**], quantum confinement due to presence of nanocrystallites [**50**], presence of oxygen and also to low density amorphous tissues and micro-voids in the film [**51**]. Recently, *Gogoi et al.* [**52**] have also reported high band gap nanocrystalline Si films prepared by HW-CVD method. We attribute increase of density of amorphous tissue (or decrease in crystalline fraction) with

increase in Xe dilution of silane may responsible for high band gap. The increase in amorphous fraction may increases void density in the films. The presence of voids lowers the absorption in the film and shifts the transmission curve towards higher photon energy. This produces higher band gap, which is estimated by extrapolation of absorption curve on the energy axis. The increase of amorphous fraction (or decrease in crystalline fraction) with increase in Xe dilution of silane, as revealed from low angle XRD, Raman spectroscopy and atomic force microscopy analysis further supports this conjecture.

Conclusion

In summary, we have investigated the effect of Xe dilution of silane on structural, optical and electrical properties of nanocrystalline Si films deposited by HW-CVD. With increase in Xe dilution of silane nanocrystalline-to-amorphous transition or amorpization has been observed in nanocrystalline Si films. The amorphization has been confirmed from dark and photoconductivity measurement, Raman spectroscopy, low angle XRD and atomic force microscopy analysis. The FTIR spectroscopy analysis showed that with increase in Xe dilution of silane, in addition to di-hydrogen, $Si\text{-}H_2$ and poly-hydrogen, $(Si\text{-}H_2)_n$ complexes, hydrogen incorporated in these films in mono-hydrogen, Si-H bonded species. The hydrogen content was found < 5 at. % over the entire range of Xe dilution of silane investigated and it increases with increase in Xe dilution of silane. On the other hand, E_{Tauc} and E_{04} show decreasing trend with increasing Xe dilution of silane. The E_{Tauc} decreases from 2.4eV to 1.9eV whereas E_{04} decreases from 2.9eV to 2.3eV. The optical band gap values estimated from E_{04} method are found higher than E_{Tauc} values calculated from Tauc's method. Finally, it has been concluded that Xe dilution of silane in HW-CVD enhances the deposition rate but has a deteriorating effect on the crystallinity of nanocrystalline Si films.

Lastly, escalation of the deposition rate with increase in xenon dilution promises a significant technological impact on fabrication of Si:H based solar cells.

Reference
1. Staebler, D; Wronski, C. *Appl. Phys. Lett.* **1977**, *31*, 292.
   DOI: 10.1063/1.89674
2. Ito, M; Koch, C; Svrcek, V; Schubert, M; Werner, J. *Thin Solid Film.* **2001**, *383*,129.
   DOI: 10.1016/S0040-6090(00)01590-X
3. Park, J; Shin, C; Park, H; Jung, J; Lee, Y; Bong, Se; Dao, Vi; Balaji, N; Yi, J. J. Nanosci. Nanotechnol; **2015**, *15(3)*, 2241
   DOI: 10.1166/jnn.2015.10241
4. Zhi, Q; Xinjian, X; Qiuyan, HaoL Di, W; Junming, X; Caichi, L. *Appl. Surf. Sci.* **2015**, *324*, 152.
   DOI: 10.1016/j.apsusc.2014.10.091
5. Kesarwani, A; Panwar, O; Tripathi, T; Dalai, M; Chockalingam, S. *Mater. Sci. Semicond. Process.* **2015**, *31*, 1.
   DOI: 10.1016/j.mssp.2014.11.015
6. Wu, B.; Tsai, H.; Wuu, S. Appl. Surf. Sci. **2015** (Article in Press)
   DOI: 10.1016/j.apsusc.2015.01.006
7. Lubianiker, Y; Cohen, J; Jin H; Abelson J; *Phys. Rev. B* **1999**, *60*, 4434.

DOI: 10.1103/PhysRevB.60.4434

8. Meaudre, M.; Meaudre, R.; Buttee, R.; Vignoli, S.; Longeaud, C.; Kleider. J.; Roca, P. *J. Appl. Phys.* **1999**, *86*, 946.
DOI: 10.1063/1.370829

9. Longeaud, C.; Kleider, J.; Roca, P.; Hamma, S.; Meaudre, R.; Meaudre, M. *J. Non-Cryst. Solid.* **1998**, *227*, 96.
DOI: 10.1016/S0022-3093(98)00217-8

10. Khan, M. A. M.; Kumar, S.; Ahamed, M. *Mater. Sci. Semicond. Process.* **2015,** *30*, 169,
DOI: 10.1016/j.mssp.2014.09.028

11. Juneja, S.; Sudhakar, S.; Gope, J.; Lodhi, K.; Sharma, M.; Kumar, S. *J. Alloys Compd.* **2015**, *643*, 94
DOI: 10.1016/j.jallcom.2015.04.077

12. Bu, Y.; Flewitt, A.; Miline, W. *Plasma Sci. Technol.* **2010**, *12*, 608
DOI: 10.1088/1009-0630/12/5/19

13. Goncalves, C.; Charvet, S.; Zeinert, A.; Clin, M.; Zellama, K. *Thin Solid Films;* **2003**, *403*, 91
DOI: 10.1016/S0040-6090(01)01553-X

14. Bhattacharya, K.; Das, D. Nanotechnology; **2007**, *18*, 415704.
DOI: 10.1088/0957-4484/18/41/415704

15. Zhou, H; Wei, D; Xu, S; Xiao, S; Xu, L; Huang, S; Guo, Y; Yan, W; Xu, M, *J. Appl. Phys.* **2011**, *110*, 023517
DOI: 10.1063/1.3605288

16. Shindo, W.; Sakai, S.; Tanaka, H.; Zhong, C.; Ohmi. T. *J. Vac. Sci. Technol. A.* **1999**, *17*, 3134
DOI: 10.1116/1.582017

17. Schropp, R.; Rath, J.; Li, H. *J. Cryst. Growth* **2009**, *311(*3), 760
DOI: 10.1016/j.jcrysgro.2008.09.155

18. Gogoi, P.; Jha, H.; Agarwal, P.; *Thin Solid Films;* **2010**, *518*, 6818
DOI: 10.1016/j.tsf.2010.06.040

19. Konagai, M.; *Thin Solid Films;* **2008**, *516*(5), 490
DOI: 10.1016/j.tsf.2007.06.043

20. Marquardt, D. *J. ; Soc. Ind. Appl. Math.* **1963**, *11(2)*, 431.
DOI: 10.1137/01110030

21. Kaneko, T.; Wakagi, M.; Onisawa, K.; Minemura, T. *Appl. Phys. Lett.* **1994**, *64*, 1865.
DOI: 10.1063/1.111781

22. He, Y.; Yin, C.; Cheng, G.; Wang, L.; Liu, X.; Hu, G.; *J. Appl. Phys.* **1994**, *75*, 797.
DOI: 10.1063/1.356432

23. Fritzsche, H.; Tanielian, M.; Tsai, C.; Gaczi, P.; *J. Appl. Phys.* **1979**, *50*, 3366.
DOI: 10.1063/1.326326

24. Swanepoel, R.; *J. Phys. E: Sci. Instrum.* **1983**, *17*, 1214.
DOI: 10.1088/0022-3735/16/12/023

25. Kang, S.; Jeon, M.; Park, J.; Lee, H.; Park, B.; Teon, J.; Yeom, G.; *J. Cryst. Growth* **2010**, *312*, 2145.
DOI: 10.1016/j.jcrysgro.2010.04.024

26. Naito, S.; Ikeda,, M.; Ito, N.; Hattori, T.; Goto, T.; *Jpn. J. Appl. Phys.* **1993**, *32(1)*, 5721.
DOI: 10.1143/JJAP.32.5721

27. Saitoh, T.; Shimada, T.; Migitaka, M.; *J. Non-Cryst. Solids* **1983**, *59(2)*, 715.
DOI: 10.1016/0022-3093(83)90271-5

28. Xu, G.; Wang, T.; Li, G.; Wang, J.; He, Y.; Ma, X.; Zheng, G. *Chin.; J. Semicond.* **2002**, *21*, 1170.

29. Droz, C.; Vallat-Sauvain, E.; Bailat, J.; Feitknecht, L.; Meier, J.; Shah, A.; *Sol. Energy Mater. Sol. Cells.* **2004**, *81(1)*, 61.
DOI: 10.1016/j.solmat.2003.07.004

30. Shindo, W.; Ohmi, T.; *J. Appl. Phys.* **1996**, *79*, 2347.
DOI: 10.1063/1.361161

31. Ino, K.; Shinohara, T.; Ushiki, T.; Ohmi, T.; *J. Vac. Sci. Technol. A* **1997**,*15(5)*, 2627.
DOI: 10.1116/1.580934

32. Zedlitz, R.; Kessler, F.; Heintze, M.; *J. Non-Cryst. Solids.* **1993**, *83*, 164.
DOI: 10.1016/0022-3093(93)90497-L

33. Hosomi, T.; Maki, T.; Kobayashi, T.; Yoshizako, Y.; Taniguchi, M.; Sugiyo, M.; *J. Appl. Phys.* **1998**, *84*, 6059.
DOI: 10.1063/1.368916

34. Wagner, S.; Wolf, S. H.; Gibson, J. M. *Mater. Res. Soc. Symp. Proc.* **1990**, *164*, 161.
DOI: 10.1557/PROC-164-161

35. Zhang, Y. F.; Zhang, F.; Gao, Q. J.; Peng, X. F.; Lin, Z.; D. *Diamond Relat. Mater.* **2001**, *10*, 1523.
DOI: 10.1016/S0925-9635(01)00383-1

36. Feenstra, K. *Ph. D. Thesis*, Utrecht University, Netherland, **1998.**

37. Bardet, E.; Bouree, J. E.; Cuniot, M.; Dixmier, J.; Elkaim, P.; Duigou, J.; Middya, A.; Perrin, J.; *J. Non-Cryst. Solids* **1996**, *198*, 867
DOI: 10.1016/0022-3093(96)00072-5

38. Wei, W.; Xub, G.; Wang, J.; Wang, T.; *Vacuum ;* **2007**, *81*, 656.
DOI: 10.1016/j.vacuum.2006.09.006

39. Lucovsky, G. *Solar Cells;* **1980**, *2*, 431.
DOI: 10.1016/0379-6787(80)90019-8

40. John, P.; Odeh, I.; Thomas, M.; *Solid State Commun.* **1982**, *41*, 341.
DOI: 10.1016/0038-1098(82)90389-1

41. Shanks, H.; Fang, C.; Cardona, M.; Desmond, F.; Kalbitzer, S.; Ley, L.; *Phys. Status Solidi B;* **1980**, *100(1)*, 43.
DOI: 10.1002/pssb.2221000103

42. Lau, W. *Infrared Characterization of Microelectronics*; World Scientific Publication: Singapore, **1999**.

43. Langford, A.; Fleet, M.; Nelson, B.; Lanford, W.; Maley, N.; Phys. Rev. B. **1992**, *45*, 13367.
DOI: 10.1103/PhysRevB.45.13367

44. Tauc, J. Amorphous and Liquid Semiconductors, Plenum Publication, London, UK, **1974**

45. Cody, G. D.; Wronski, C. R.; Abeles, B.; Stephens, R. B.; Brooks, B.; *Sol. cells* **1980**, *2*, 227.
DOI: 10.1016/0379-6787(80)90028-9

46. Horbach, C.; Beter, W.; Wagner, H.; *J. Non-Cryst. Solids* **1991**, *137*, 661.
DOI: 10.1016/S0022-3093(05)80207-8

47. Wallinga, J.; Arnoldbik, W. M.; Vredenberg, A. M.; Schropp, R. E. I.; Van der Weg, W. F.; *J. Phys. Chem. B* **1998**, *102*, 6219.
DOI: 10.1021/jp981447l

48. Kumar, S.; Dixit, P.; Rauthan, M.; Parashar, A.; Jhuma, G.; *J. Phys., Condens. Matter* **2008**, *20*, 335215.
DOI: 10.1088/0953-8984/20/33/335215

49. Mahan, A.; Biswas, R.; Gedvilas, L.; Williamson, G.; Pan, B.; *J. Appl. Phys.* **2004**, *96*, 3818.
DOI: 10.1063/1.1772876

50. Furukawa, S.; Miyasato, T.; *Phys. Rev. B.* **1988**, *38(8)*, 5726.
DOI: 10.1103/PhysRevB.38.5726

51. Janssen, R.; Jannota, A.; Dimova-malinovska, D.; Stutzmann, M.; *Phys. Rev. B.* **1999**, *60*, 13561.
DOI: 10.1103/PhysRevB.60.13561

52. Gogoi, P.; Jha, H.; Agarwal, P.; *Thin Solid Films.* **2010**, *518*, 6818.
DOI: 10.1016/j.tsf.2010.06.040